ЖЭТФ, 2005, том 127, вып. 4, стр. 860–876

HIGH-PRESSURE HYDROGENATED FULLERENES: OPTICAL SPECTRA AND STABILITY OF $C_{60}H_{36}$ AT HIGH PRESSURE

K. P. Meletov*

Institute of Solid State Physics, Russian Academy of Sciences
142432, Chernogolovka, Moscow Region, Russia

G. A. Kourouklis

Physics Division, School of Technology, Aristotle University of Thessaloniki
GR-540 06, Thessaloniki, Greece

Submitted 14 October 2004

The optical Raman and photoluminescence (PL) spectra of the high-pressure hydrogenated fullerene C_{60} are studied at normal conditions and at high pressure. The Raman spectrum of the most stable hydrofullerene $C_{60}H_{36}$ contains a large number of peaks related to various isomers of this molecule. Comparison of the experimental data with the results of calculations shows that the most abundant isomers have the symmetries S_6, T, and D_{3d}. The Raman spectrum of deuterofullerene $C_{60}D_{36}$ is similar to that of $C_{60}H_{36}$, but the frequencies of the C–H stretching and bending modes are shifted due to the isotopic effect. The PL spectrum of hydrofullerene $C_{60}H_{36}$ is shifted to higher energies by approximately 1 eV with respect to that of pristine C_{60}. The effect of hydrostatic pressure on the Raman and PL spectra of $C_{60}H_{36}$ has been investigated up to 12 GPa. The pressure dependence of the phonon frequencies exhibits peculiarities at approximately 0.6 GPa and 6 GPa. The changes observed at approximately 0.6 GPa are probably related to a phase transition from the initial orientationally disordered body-centered cubic structure to an orientationally ordered structure. The peculiarity at approximately 6 GPa may be related to a pressure-driven enhancement of the C–H interaction between the hydrogen and carbon atoms belonging to neighboring molecular cages. The pressure-induced shift of the photoluminescence spectrum of $C_{60}H_{36}$ is very small up to 6 GPa, and a negative pressure shift was observed at higher pressure. All the observed pressure effects are reversible with pressure.

PACS: 61.48.+c, 62.50.+p, 64.70.Kb, 78.30.Na, 78.55.Kz

1. INTRODUCTION

Hydrofullerenes have attracted considerable interest, particularly in relation to their potential use as hydrogen storage materials [1]. The existence of several hydrofullerenes has been predicted by theoretical calculations and some of them have been synthesized [2–5]. The most stable member, $C_{60}H_{36}$, is the hydrogenated derivative of the pristine C_{60} molecule, which can be prepared using either the high-pressure hydrogenation [6] or the hydrogen-atom transfer to C_{60} from other reagents in solution [7]. The hydrofullerene samples prepared by the use of both methods are usually rather nonuniform and may contain hydrides with various mass weights, as well as a small amount of reagents. Characterization of the hydrogenation reaction products is therefore of great importance and various methods like the electron, X-ray, and neutron diffraction, nuclear magnetic resonance, infrared spectroscopy, and laser desorption mass spectrometry have been used for this purpose [4–6, 8–10].

The $C_{60}H_{36}$ molecule could exist in a great number of isomeric forms, but only a small number of them are stable [11]. The isomeric form with the highest symmetry, T_h, has 12 double bonds, arranged as far apart as possible on its surface, while the form having the double bonds in four isolated aromatic six-member rings lacking hydrogen atoms and located at the corners of a tetrahedron has a T-symmetry structure. Between these two extremes are the isomers with the symmetry D_{3d} and S_6, which have two six-member rings at the three-fold axis poles of the molecule, with the other six

*E-mail: mele@issp.ac.ru

double bonds isolated in six pentagons. The presence of various isomers in the $C_{60}H_{36}$ specimens depends most likely on the preparation method and on the kinetic parameters controlling the hydrogen addition reaction. Thus, $C_{60}H_{36}$ prepared by transfer hydrogenation of C_{60} contains a mixture of the principal isomers D_{3d} and S_6, while $C_{60}H_{36}$ prepared by zinc reduction of C_{60} in aromatic solvents contains the S_6 isomer as the most abundant [12–14]. Concerning the solid-state phase of $C_{60}H_{36}$, Hall et al. [9] have suggested the body-centered cubic structure (BCC) with the cell parameter 11.785 ± 0.015 Å for the packing of the molecules in the crystalline state. Furthermore, they suppose, at least for the D_{3d} isomer, that the BCC crystal structure transforms into a body-centered tetragonal one at low temperatures.

The optical characterization of hydrofullerenes is of great importance and the Raman scattering was successfully used for the study of the vibrational spectrum of $C_{60}H_{36}$ prepared by the transfer hydrogenation method [12]. The incorporation of 36 hydrogen atoms in the C_{60} cage lowers the molecular symmetry and activates Raman scattering from a variety of the initially forbidden phonon modes. In addition, the appearance of the C–H stretching and bending modes and those related to various isomers of $C_{60}H_{36}$ results in a very rich Raman spectrum [12]. The comparison of the phonon frequencies for five principal isomers of $C_{60}H_{36}$ obtained by molecular dynamics calculations with the experimentally observed phonon frequencies has led to the conclusion that the material prepared by the transfer hydrogenation method mainly contains two isomers, those with the symmetries D_{3d} and S_6 [12].

In this paper, we study the optical Raman and PL spectra of the hydro- and deuterofullerene, $C_{60}H_{36}$ and $C_{60}D_{36}$, respectively, prepared by high-pressure hydrogenation. The aim of the research was to identify the phonon and electron energy spectra of the high-pressure hydrogenated fullerene, to clarify the isomer composition and homogeneity of samples, and to study the isotopic effects in the vibrational spectra. The Raman spectra of the high-pressure hydrogenated samples were compared with those obtained by transfer hydrogenation and with the molecular dynamics calculation data [12]. The Raman data show the presence of all principal isomers in the high-pressure hydrogenated fullerenes and a large isotopic shift for the C–H stretching mode, whereas the shift of the modes related to the fullerene molecular cage is negligible. We have also studied the pressure behavior of the Raman and PL spectra of $C_{60}H_{36}$ at pressure up to 12 GPa in order to obtain information about the structural and chemical stability of the material at high pressure. The incorporation of hydrogen in the fullerene molecular cage may play an important role in the stability of the material, in particular, may prevent the pressure-induced polymerization that is typical of pristine C_{60} under high-pressure and high-temperature treatment [15]. The hydrogen incorporation may also affect the pressure-induced phase transition of the rotational disorder/order nature in analogy to the case of pristine C_{60}. We have studied the pressure behavior of phonon frequencies and the pressure-induced shift of electronic bands. The pressure coefficients of the phonon modes are positive and demonstrate singularities at approximately 0.6 and 6 GPa. The pressure shift of the luminescence spectrum is unusually small and increases somehow at $P \geq 6$ GPa. All the observed features are reversible with pressure and $C_{60}H_{36}$ is stable in the pressure region investigated.

2. EXPERIMENTAL DETAILS

The commercial material, C_{60} of 99.99 % purity, was sublimed twice in vacuum better than 10^{-5} Torr at 800 K, and was then compacted into pellets of 12 mm diameter and 1 mm thickness. Each pellet was placed into a copper capsule, covered with a disc of 0.01-mm thick Pd foil, and then annealed in vacuum at 620 K for 2 h to expel desorbed gases. The remaining volume in the capsule was filled with AlH_3 or AlD_3 for hydrogenation or deuteration, respectively, and was then tightly plugged with a copper lid using gallium as solder. This encapsulation procedure effectively prevents hydrogen or deuterium losses during subsequent treatment, because both Cu and Ga are largely impermeable by hydrogen.

The assembled capsules were pressurized to 3.0 GPa in a toroid-type high-pressure cell and maintained at 650 ± 10 K or 700 ± 10 K for a time of 24 or 48 h. AlH_3 decomposes above 400 K [16], producing hydrogen reacting with the fullerite after permeating the Pd foil, which isolates the fullerite from chemically active Al. The amount of the hydrogen gas produced inside the capsule corresponds to the particle ratio $H/C_{60} \approx 90$. Therefore, the available hydrogen quantity is always in excess of the C_{60} particle number during the hydrogenation experiments. The hydrogenation procedure was repeated for a second run, with the product of the first run taken as a starting material for the second run. Preliminary mass-spectrometry data show that at least 95 % of the material in the capsule is hydrofullerene $C_{60}H_{36}$, while the remaining 5 % contains par-

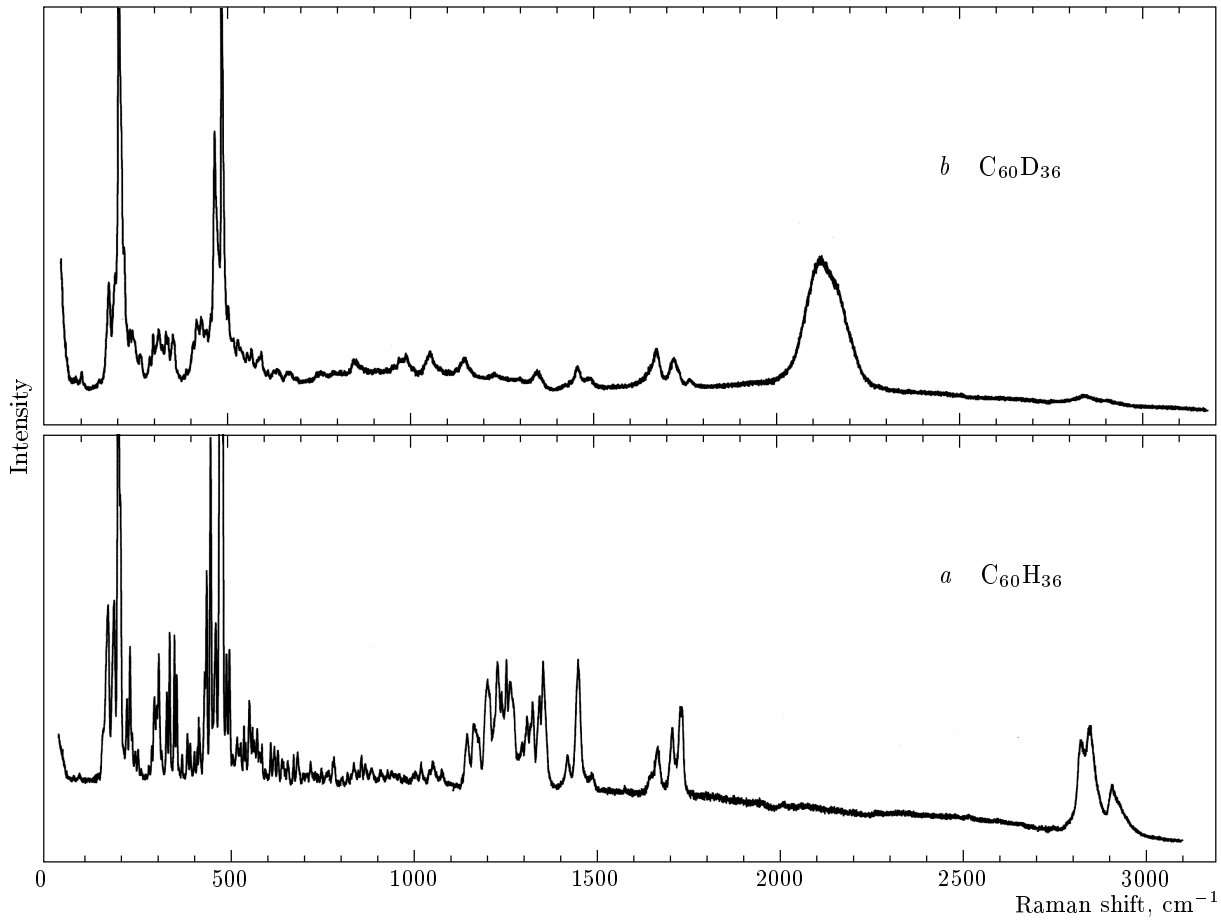

Fig. 1. Raman spectra of the $C_{60}H_{36}$ (a) and $C_{60}D_{36}$ (b) samples taken at ambient conditions in the energy range 50–3100 cm^{-1}. The samples were prepared by means of high-pressure hydrogenation at $P = 3.0$ GPa, $T = 700$ K, and reaction time approximately 24 hours

tially hydrogenated fullerenes. The X-ray analysis of the obtained material shows that it has the BCC structure, typical of $C_{60}H_{36}$ [9], with the lattice parameter 11.83 Å.

For the optical measurements, visually uniform, colorless, and transparent specimens were selected. Raman spectra were recorded using a triple monochromator DILOR XY-500 equipped with a CCD liquid-nitrogen cooled detector system. The spectra were taken in the backscattering geometry by the use of the micro-Raman system comprising an OLYMPUS microscope equipped with an MSPlan100 objective with magnification 100 and spatial resolution approximately 1.7 μm. The spectral width of the system was approximately 2.0 cm^{-1}. The Raman frequencies were calibrated by the use of the low-pressure Ne lamp with the accuracy better than 0.2 cm^{-1}. To avoid interference from luminescence, the sample was excited by the 676.4 nm line of the Kr^+ laser, whose energy is below the fundamental absorption gap of the material. The laser power was varied from 5 to 10 mW, measured directly before the sample, to avoid the destruction of the samples by laser heating. The phonon frequencies were obtained by fitting Gaussian line shapes to the experimental Raman spectra. The PL spectra were recorded using a single monochromator JOBIN YVON THR-1000 equipped with a CCD liquid-nitrogen cooled detector system. The 457.9 nm line of an Ar^+ laser was used for excitation of the luminescence spectra. The laser power was about 2 mW measured directly in front of the high-pressure cell; the spectral width of the system was approximately 1.0 cm^{-1}. The measurements at high pressure were carried out using the diamond anvil cell (DAC) of Mao Bell type [17]. The 4 : 1 methanol–ethanol mixture was used as a pressure-transmitting medium and the ruby fluorescence

technique was used for pressure calibration [18]. The samples used for the high-pressure measurements had typical dimensions of approximately 100 μm.

3. RESULTS AND DISCUSSION

3.1. Isomeric composition and isotopic effect in $C_{60}H_{36}$

The Raman spectra of $C_{60}H_{36}$ and $C_{60}D_{36}$ taken in the frequency region 50–3150 cm^{-1} at ambient conditions are shown in Fig. 1*a* and Fig. 1*b*, respectively. Both samples were synthesized at the pressure 3.0 GPa, temperature 700 K and reaction time approximately 24 hours. The spectrum in Fig. 1*a* consists of 126 sharp peaks with the lowest mode located at 86 cm^{-1} and the highest at 2912 cm^{-1}. For comparison, the Raman spectrum of pristine C_{60} contains only ten active modes, $H_g(1) - H_g(8)$ and $A_g(1) - A_g(2)$, with frequencies located in the region 273–1726 cm^{-1} [19]. The spectrum in Fig. 1*a* was taken at the best site of the best sample, selected from the content of the ampoule by preliminary micro-Raman probing as having the lowest background and the clearest Raman signal. A number of rather good samples, taken from the same ampoule, show the Raman peaks less intense with respect to the relatively large background. The higher background is probably a result of a higher concentration of structural defects and impurities in the sample under study. These impurities may be microscopic amounts of partially hydrogenated fullerenes, which are fluorescing under Kr-laser excitation in the spectral region under investigation. The majority of the selected samples from the content of the ampoule show the Raman signal similar to that of the best one, but there are also many samples that give a large background obscuring the structure of the Raman spectrum. The samples obtained by high-pressure hydrogenation are rather nonuniform and great care should be exercised during the sample selection. Using the micro-Raman probe, we have checked a number of samples from different ampoules in order to examine their quality in relation to the hydrogenation parameters, namely, temperature and reaction time. The results show that the sample quality does not depend significantly on the reaction time; on the contrary, temperature drastically affects their optical quality. Samples hydrogenated at 700 K show a better optical quality and their Raman spectra show a rich structure, well-resolved intense peaks, and relatively small background.

The Raman spectrum of $C_{60}H_{36}$ differs drastically from that of pristine C_{60}. The most important differences in their spectra are as follows:

i) the number of the Raman-active modes increases dramatically,

ii) the low-energy radial modes (200–600 cm^{-1}) exhibit a considerable intensity enhancement with respect to the high-energy tangential modes (1400–1700 cm^{-1}). In addition, a number of new modes appear that are related to the C–H bending (1150–1350 cm^{-1}) and stretching (2800–3000 cm^{-1}) vibrations.

The vibrational data related to the Raman spectrum of $C_{60}H_{36}$ are summarized in Table 1. The first three columns of Table 1 contain the data related to the number, position, and intensity of the Raman peaks. The next two columns contain experimental results related to the positions and intensities of the Raman peaks of $C_{60}H_{36}$ reported in previous studies [12, 13]. The last three columns of Table 1 are related to the frequency, Raman cross section, and symmetry of the Raman-active modes of various isomers of the $C_{60}H_{36}$ molecule according to calculations [12] using the modified MNDO method. The comparison of the present experimental data with those in Refs. [12, 13] shows that the Raman spectrum of high-pressure hydrogenated $C_{60}H_{36}$ is more than five times richer than that of transfer hydrogenated $C_{60}H_{36}$. The majority of the experimentally observed Raman peaks (86 peaks from a total number of 126) are very close, to an accuracy of approximately 5 cm^{-1}, to the calculated frequencies and cross sections of the Raman-active modes (their total number is approximately 400) [12]. The peaks that are close to the calculated frequencies are assigned to all principal isomers, but a majority of them belong to isomers with the symmetries S_6, T, and D_{3d}. We emphasize that the complexity of the calculated vibrational spectrum, the large number of isomers, and the accuracy of the molecular dynamics calculations might sometimes result in an accidental agreement (disagreement) of the experimental and calculated data. The peaks that are rather far from the calculated Raman frequencies belong mainly to the low-energy radial modes of the fullerene cage and are probably related to the presence of other isomers of $C_{60}H_{36}$ in the samples under study.

The Raman spectrum of deuterofullerene $C_{60}D_{36}$, taken at ambient conditions, is shown in Fig. 1*b*. A first glance at the Raman spectra of hydro- and deuterofullerene indicates that they have several similarities, but an important difference is also apparent. The spectrum is less rich in structure than that of $C_{60}H_{36}$. It contains about 80 peaks, probably due to a different isomer composition of $C_{60}D_{36}$ samples. The positions

Table 1. Frequencies and intensities of the observed and calculated Raman peaks in $C_{60}H_{36}$

Experiment					Theory		
Present work			Ref. [12]	Ref. [13]	Ref. [12]		
№	ω, cm^{-1}	Intensity*	ω, cm^{-1}	ω, cm^{-1}	ω, cm^{-1}	$\sigma^{\dagger}$	Isomer
1	86.0	vw	85				
2	101.1	w		128			
3	165.7	m	136				
4	176.6	vs	175	180	176	7	T
5	192.3	s			194	7	D_{3d}
6	196.9	vs			198	14	T_h
7	206.6	vs		207	206	21	T
8	212.4	vs	211		214	22	T_h
9	230.6	s			229	18	D_{3d}
10	239.3	s		239			
11	245.3	m					
12	253.6	m					
13	261.3	m	264				
14	291.0	m					
15	298.7	s			294	11	T
16	305.5	s					
17	311.8	m	313				
18	317.8	s					
19	326.4	m			325	3	D_{3d}
20	339.6	s			341	14	D_{3d}
21	347.2	s			346	8	S_6
22	360.3	s			365	10	S_6
23	366.9	s			367	10	$D_{3d}(c-k)$
24	381.8	m			379	1	T
25	396.3	s	395	395	395	7	D_{3d}
26	404.3	m			404	2	D_{3d}
27	415.3	m			415	7	$D_{3d}(c-k)$
28	423.0	m			422	9	S_6
29	429.4	m			427	4	D_{3d}
30	443.0	s		444	442	3	T
31	448.4	vs	448				
32	458.6	vs		458	460	17	S_6
33	465.6	s			465	1	D_{3d}
34	473.2	s			473	1	T
35	484.4	vs	484	484	488	44	T
36	491.3	vs			496	14	S_6
37	501.9	s					
38	509.9	s			509	31	S_6

Table 1.

Experiment					Theory		
Present work			Ref. [12]	Ref. [13]	Ref. [12]		
№	ω, cm^{-1}	Intensity*	ω, cm^{-1}	ω, cm^{-1}	ω, cm^{-1}	$\sigma^{\dagger}$	Isomer
39	522.0	m			522	1	T
40	531.0	m					
41	537.0	m					
42	541.4	m			545	1	T
43	549.9	s					
44	554.9	m					
45	565.0	s			569	14	T
46	573.1	m			570	11	$D_{3d}(c-k)$
47	577.6	m			579	30	S_6
48	580.6	m			581	7	S_6
49	585.7	s			586	6	D_{3d}
50	590.7	m					
51	596.3	m			597	52	$D_{3d}(c-k)$
52	622.6	w					
53	632.4	w			634	1	$D_{3d}(c-k)$
54	642.5	w			647	2	S_6
55	653.3	w			653	3	T
56	657.7	w					
57	662.0	w			663	1	D_{3d}
58	669.5	w			671	4	S_6
59	685.0	m					
60	696.3	w			699	11	D_{3d}
61	711.6	m					
62	720.6	m			719	4	T
63	731.6	m			731	36	D_{3d}
64	744.5	w					
65	752.3	w		753			
66	761.1	w					
67	774.2	w					
68	781.3	w					
69	791.3	m			796	2	T_h
70	795.9	m			796	4	D_{3d}
71	817.2	w					
72	832.4	w			828	1	T
73	849.5	m			852	7	S_6
74	861.7	w			860	2	T
75	869.2	m					
76	880.4	m			875	2	T

Table 1.

Experiment					Theory		
Present work			Ref. [12]	Ref. [13]	Ref. [12]		
№	ω, cm^{-1}	Intensity*	ω, cm^{-1}	ω, cm^{-1}	ω, cm^{-1}	$\sigma^{\dagger}$	Isomer
77	922.2	w			921	3	T_h
78	940.2	w			939	1	T
79	951.1	w			948	1	S_6
80	960.8	w			959	5	T_h
81	972.3	w			972	1	T
82	985.6	vw					
83	991.4	w			988	5	T_h
84	1015.1	w	1015	1008	1018	2	S_6
85	1032.4	m	1039	1039			
86	1054.1	w			1053	4	S_6
87	1064.0	m					
88	1073.2	w			1073	2	T_h
89	1088.6	w			1087	1	S_6
90	1125.2	w			1126	1	T_h
91	1154.0	m	1154		1154	16	$D_{3d}(c-k)$
92	1173.9	m			1172	18	T
93	1181.3	m			1182	12	T
94	1189.7	m		1186	1191	2	D_{3d}
95	1207.7	m			1209	9	D_{3d}
96	1212.6	s	1212	1213	1213	44	T_h
97	1218.7	s			1217	23	S_6
98	1227.2	m			1228	5	T
99	1231.8	m			1232	1	S_6
100	1240.3	s			1238	36	T
101	1250.3	s			1252	22	$D_{3d}(c-k)$
102	1256.9	m			1258	19	S_6
103	1263.2	s		1262	1263	42	D_{3d}
104	1274.0	s	1276		1274	74	D_{3d}
105	1283.8	m			1284	12	$D_{3d}(c-k)$
106	1306.1	w			1304	2	S_6
107	1314.4	m			1313	29	T_h
108	1319.6	s			1318	22	$D_{3d}(c-k)$
109	1328.3	m			1326	33	S_6
110	1334.9	s			1330	27	S_6
111	1348.3	m					
112	1353.2	s					
113	1362.9	s			1363	9	D_{3d}
114	1369.4	m	1386		1370	11	S_6

Table 1.

Experiment					Theory		
Present work			Ref. [12]	Ref. [13]	Ref. [12]		
№	ω, cm^{-1}	Intensity*	ω, cm^{-1}	ω, cm^{-1}	ω, cm^{-1}	$\sigma^{\dagger}$	Isomer
115	1430.6	m		1402	1429	5	D_{3d}
116	1457.0	s	1462	1462			
117	1496.6	w	1508	1497			
118	1653.8	w					
119	1674.8	m			1671	401	S_6
120	1714.0	s	1714		1712	211	$D_{3d}(c-k)$
121	1724.5	w					
122	1739.4	s	1736		1739	333	$D_{3d}(c-k)$
123	2826.8	s	2830	2829			
124	2852.5	s	2853	2852	2856	55	D_{3d}
125	2911.9	s	2913	2911	2911	180	D_{3d}
126	2931.2	m				8	

$D_{3d}(c-k)$ — the lowest energy isomer with D_{3d} symmetry [13].
*Intensity characterization: very weak (vw), weak (w), medium (m), strong (s), and very strong (vs).
†Raman cross section (Å^4/amu) [12].

Table 2. Molecular cage vibrations and C–H stretching modes with their isotopic shift ratio

$C_{60}H_{36}$		$C_{60}D_{36}$			
Ω, cm^{-1}	Intensity*	Ω, cm^{-1}	Intensity*	Ω_H/Ω_D	$(\Omega_H/\Omega_D)^2$
206.6	vs	203.4	vs	1.016	1.032
212.4	vs	209.7	vs	1.013	1.026
464.2	vs	464.2	vs	1	1
484.4	vs	484.4	vs	1	1
2826.8	s	2113.6	s	1.337	1.789
2852.5	s	2169.7	s	1.315	1.728
2911.9	s	2209.3	s	1.318	1.737

*Intensity characterization: strong (s) and very strong (vs).

of the C–D stretching modes are shifted towards lower energies with respect to the C–H stretching modes. The related Raman peaks are located in the frequency regions 2113–2209 cm^{-1} and 2827–2912 cm^{-1} for $C_{60}D_{36}$ and $C_{60}H_{36}$, respectively. A similar shift is also observed for the C–D bending modes, which are located in the frequency regions 800–1200 cm^{-1} and 1150–1350 cm^{-1} for $C_{60}D_{36}$ and $C_{60}H_{36}$, respectively. We note that the Raman spectrum of $C_{60}D_{36}$ also contains several very weak peaks near 2900 cm^{-1}, which are coincident with the C–H stretching modes of $C_{60}H_{36}$. This is related to the isotopic contamination of the samples under study, which contain a small amount of $C_{60}H_{36}$ caused by initial isotopic contamination of the deuterium provider (AlD_3) used for the high-pressure synthesis.

The shift of the C–H stretching and bending modes is related to the isotopic effect on the vibrational frequencies caused by substitution of hydrogen by deuterium. The isotopic shift of the stretching mode fre-

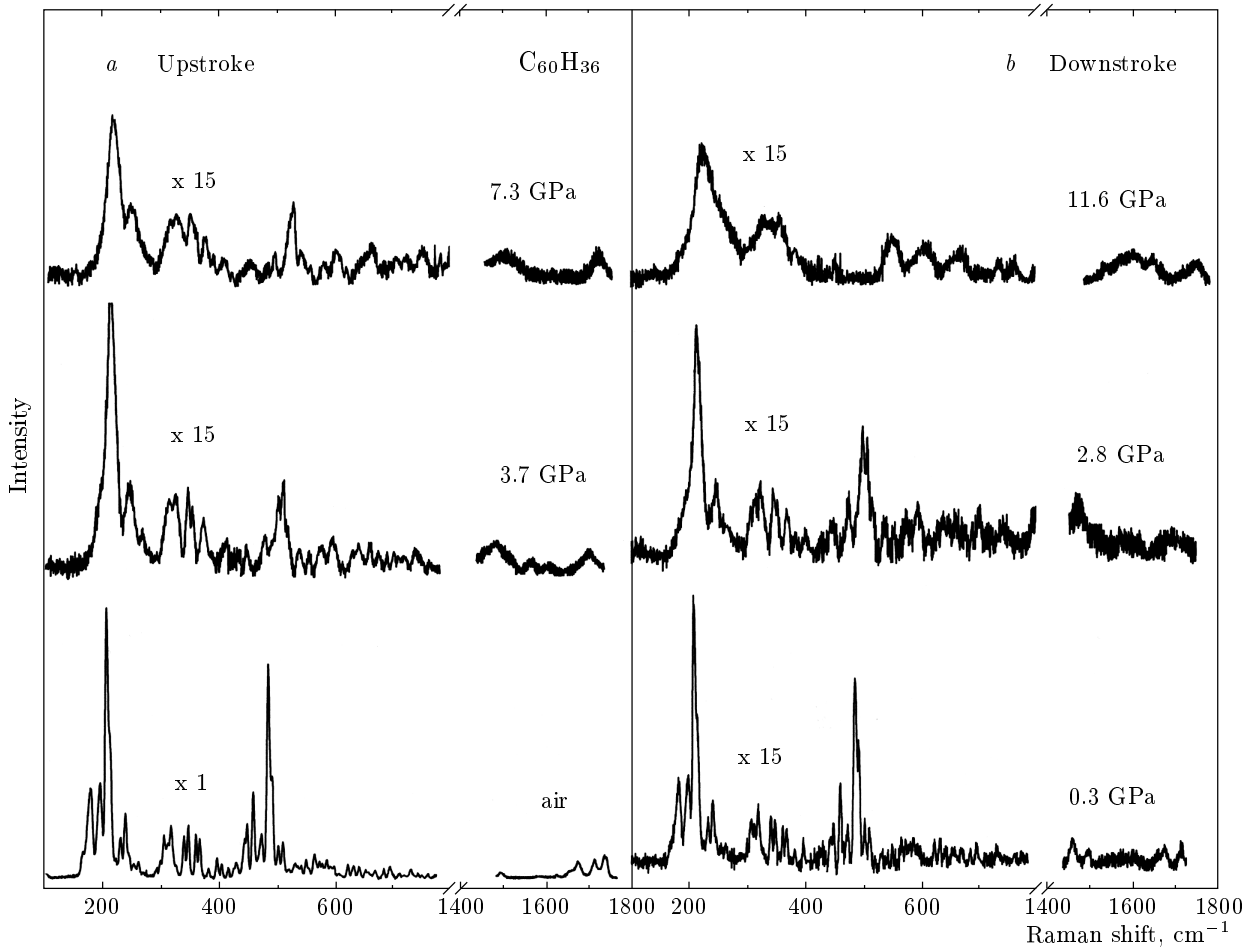

Fig. 2. Raman spectra of $C_{60}H_{36}$ recorded at room temperature during the increasing (a) and decreasing (b) pressure cycle in the frequency range 100–1800 cm^{-1}. The frequency range containing the strong diamond Raman line is excluded

quencies can be estimated from the formula

$$\frac{\Omega_H}{\Omega_D} \sim \left(\frac{M_{\Omega H}}{M_{\Omega D}}\right)^{1/2}, \qquad (1)$$

where Ω_H and Ω_D are the respective frequencies of the $C_{60}H_{36}$ and $C_{60}D_{36}$ molecules and $M_{\Omega H}$ and $M_{\Omega D}$ are the reduced masses involved in the vibrations. The large difference between the masses of the hydrogen atom and the C_{60} molecule indicates that the C–H stretching mode is mainly related to displacements of the hydrogen atom along the bond direction, whereas the C_{60} molecule remains practically stationary. Thus, the isotopic shift of the C–H stretching mode is expected to be close to the square root of the deuterium-to-hydrogen mass ratio. The same is also expected for the isotopic shift of the C–H bending mode. The frequencies and isotopic shifts of a number of intense modes related to the fullerene cage vibrations and to the C–H stretching vibrations are tabulated in Table 2. The largest isotopic shifts $[\Omega_H/\Omega_D]^2$ were observed for the C–H stretching modes that vary in the region 1.73–1.79. These values are close to the mass ratio of deuterium and hydrogen, $M_D/M_H = 2$. The isotopic shift for the modes related to the fullerene cage vibrations is small with respect to the C–H stretching modes and varies within 1–1.032. The difference in the isotopic shifts between the stretching modes and the fullerene cage modes is related to the fact that the hydrogen atoms do not participate essentially in the cage vibrations. These results are very close to those obtained by means of surface-enhanced Raman scattering of hydrogen and deuterium chemisorbed on a diamond (100) surface [21]. The frequencies of the C–H and C–D stretching modes in Ref. [21] are equal to 2830, 2865, 2928 cm^{-1} and 2102, 2165, 2195 cm^{-1}, respectively, and the isotopic shift varies within 1.32–1.35. Thus,

the parameters of the C–H stretching modes of hydrofullerene could be similar to those of hydrogen, bonded with carbon atoms on the diamond surface. This similarity is related to the large difference between the masses of the hydrogen atom and the fullerene molecule or the carbon network in diamond. In addition, the C–H bonding in both cases takes place with sp^3 coordinated carbon atoms.

3.2. Pressure behavior of Raman spectra and stability of $C_{60}H_{36}$ at high pressure

The Raman spectra of $C_{60}H_{36}$ recorded in the regions 100–800 cm^{-1} and 1400–1750 cm^{-1} at room temperature and high pressure are shown in Fig. 2 for increasing (a) and decreasing (b) pressure runs, respectively. The Raman modes appearing in this frequency region are related mainly to the vibrations of the fullerene molecular cage. The spectral region where the strong diamond vibration is located is excluded. As can been seen from Fig. 2, a rich Raman spectrum, with well-defined structures in the low-frequency region, can easily be followed with pressure. On the contrary, the structures in the spectral region 1400–1750 cm^{-1} are broad and weak, but still they can be traced up to the highest pressure studied. At first glance, the application of pressure seems to have the expected effect in the Raman spectrum, i.e., an overall positive shift in the frequencies of the Raman modes and a relative increase in their line widths. But the situation differs significantly for the part of the Raman spectrum containing the hydrogen stretching vibrations. As can be seen in Fig. 3, where the C–H stretching vibrations are presented, the initially well-separated structures in the corresponding spectra are gradually washed out, becoming a very broad structure for pressures higher than approximately 2.0 GPa. We note that despite considerable broadening of the Raman structures, the pressure effect is fully reversible upon releasing pressure, as can be seen from Fig. 2 and the top frame in Fig. 3.

The pressure dependence of the Raman frequencies is shown in Figs. 4 and 5 for pressure up to 12 GPa and at room temperature. The different open (solid) symbols correspond to pressure increase (decrease) in different pressure runs, while the solid lines through the experimental points represent linear least-square fittings. The shaded areas near the pressure approximately 0.6 and 6.0 GPa denote the pressure regions where the change in the slope of the pressure dependence or the disappearance of some Raman peaks occur. The parameters of linear least-square fittings and a tentative mode assignment of the observed Raman modes are compiled in Table 3. In the mode assignment column, we indicate the isomeric form to which this mode most likely belongs. The data related to pristine C_{60} are also included in Table 3 for comparison. The pressure dependence presented in Figs. 4 and 5 and numerical data in Table 1 show that all the observed modes have positive pressure coefficients and at least four Raman peaks disappear for pressures higher than approximately 6 GPa. Furthermore, the majority of Raman modes exhibit a change in the slope of their pressure dependence at approximately 0.6 and near the pressure of approximately 6 GPa. These peculiarities were observed for both increasing and decreasing pressure runs, and therefore the pressure dependence of the Raman mode frequencies exhibits fully reversible behavior.

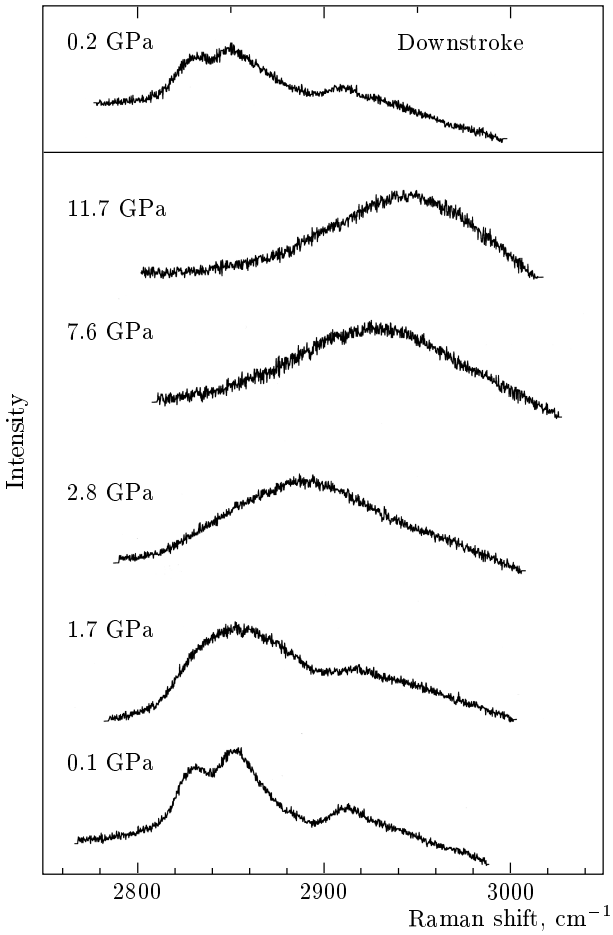

Fig. 3. Raman spectra of $C_{60}H_{36}$ recorded in the frequency range of the C–H stretching mode at ambient temperature and various pressures for increasing pressure. The spectrum in the upper frame, at 0.2 GPa, is recorded upon pressure release

The pressure dependence of the stretching C–H vi-

Table 3. The phonon frequency assignment and their pressure coefficients for the $C_{60}H_{36}$ Raman-active modes. The corresponding values for C_{60} are also included for comparison

	$C_{60}H_{36}$				C_{60}^a	
Mode		0–0.6 GPa	0.6–6 GPa	6–12 GPa	0.4–2.4 GPa	
	ω, cm^{-1}	$\partial\omega_i/\partial P$, cm^{-1}/GPa	$\partial\omega_i/\partial P$, cm^{-1}/GPa	$\partial\omega_i/\partial P$, cm^{-1}/GPa	ω, cm^{-1}	$\partial\omega_i/\partial P$, cm^{-1}/GPa
$T_g(T)$	180.6	5.6 ± 0.1	6.4 ± 0.1			
$E_g(T_h)$	196.0	4.7 ± 0.6	3.1 ± 0.4	0.6 ± 0.1		
$E_g(T)$	206.6	2.7 ± 0.3	2.2 ± 0.1	1.6 ± 0.1		
$T_g(T_h)$	212.6	2.3 ± 0.3	2.6 ± 0.1	1.7 ± 0.2		
$E_g(D_{3d})$	230.6	3.5 ± 0.1	2.9 ± 0.1	1.2 ± 0.2		
	239.1	3.2 ± 0.2	2.6 ± 0.2	1.5 ± 0.2		
	261.1	2.1 ± 0.1	1.3 ± 0.1	0.4 ± 0.2	$272 H_g(1)$	3.2
	305.2	2.2 ± 0.2	1.8 ± 0.2	1.2 ± 0.2	$294\omega_1$	2.5
	317.8	3.1 ± 0.1	1.9 ± 0.1	1.0 ± 0.2		
$E_g(D_{3d})$	339.6	2.1 ± 0.1	1.4 ± 0.1	0.9 ± 0.1		
$A(S_6)$	347.1	2.7 ± 0.1	1.6 ± 0.1	1.1 ± 0.1	$345\omega_2$	2.9
$E_g(T_h)$	366.7	3.2 ± 0.2	0.5 ± 0.2	1.7 ± 0.3		
$A_g(T)$	484.2	4.6 ± 0.2	0.5 ± 0.2	3.3 ± 0.2		
$A_g(S_6)$	491.0	3.3 ± 0.1	2.7 ± 0.1		$495 H_g(2)$	4.2
	501.8	2.0 ± 0.1	2.7 ± 0.1	3.3 ± 0.1		
$E_g(S_6)$	530.6	2.7 ± 0.2	1.7 ± 0.2	2.4 ± 0.2	$522\omega_5$	1.0
$E_g(D_{3d})$	585.7	2.6 ± 0.2	2.0 ± 0.2	0.9 ± 0.2		
$E_g(S_6)$	598.6	2.3 ± 0.2	1.9 ± 0.2	0.9 ± 0.2		
$T_g(T_h)$	622.6	2.9 ± 0.2	2.0 ± 0.2	2.3 ± 0.2	$624\omega_1$	1.5
$E_g(D_{3d})$	632.5	2.4 ± 0.1	2.0 ± 0.1	2.1 ± 0.3		
$E_g(D_{3d})$	642.5	1.9 ± 0.2	1.5 ± 0.2	2.5 ± 0.2		
$T_g(T)$	655.8	1.2 ± 0.2	1.7 ± 0.2	1.2 ± 0.2		
$E_g(T_h)$	669.3	1.9 ± 0.1	1.3 ± 0.1			
$A_{1g}(D_{3d})$	695.6	1.8 ± 0.1	1.6 ± 0.1	2.0 ± 0.4		
$A_{1g}(D_{3d})$	730.9	1.4 ± 0.2	2.5 ± 0.2	2.3 ± 0.2	$729\omega_8$	-2.9
$T_g(T)$	1459.5	9.0 ± 0.2	6.6 ± 0.2	4.4 ± 0.4	$1467 A_g(2)$	5.5
$E_g(S_6)$?	1494.5	9.6 ± 0.3	4.8 ± 0.3	5.1 ± 0.4		
$A_g(S_6)$	1674.6	4.6 ± 0.3	7.2 ± 0.3	6.9 ± 0.4		
$A_g(T_h)$	1712.5	5.2 ± 0.3	3.6 ± 0.3	2.8 ± 0.5		

[a] Data taken from Ref. [35].

brations, where a dramatic broadening occurs with increasing pressure, is the most striking pressure effect on the Raman spectra of $C_{60}H_{36}$. In our opinion, the abnormal broadening of the initially sharp peaks in the Raman spectra of $C_{60}H_{36}$ may be related to the presence of various isomers in the samples under study. Numerical calculations in Ref. [12] show that there are many identical Raman modes related to various isomers of $C_{60}H_{36}$ with very close frequencies. We believe that any difference in their pressure coefficients, even small,

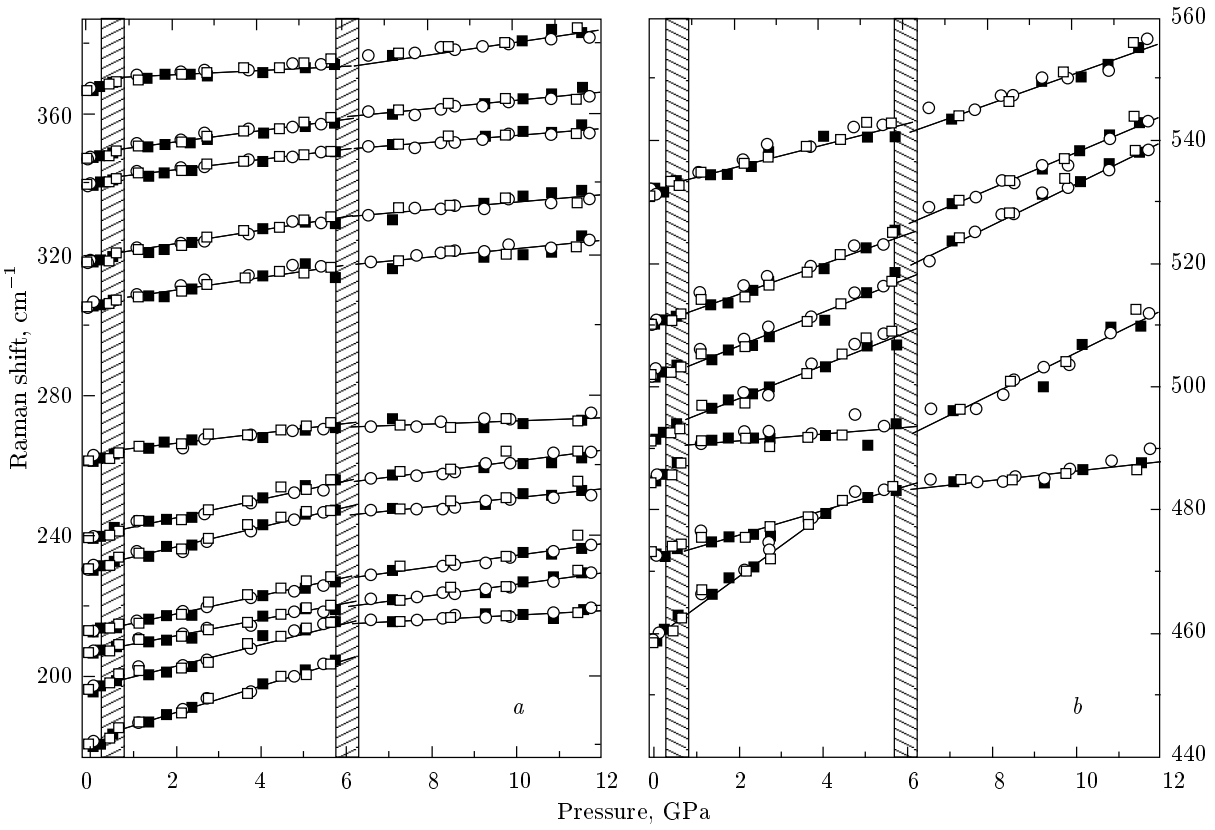

Fig. 4. Pressure dependence of Raman-active modes of $C_{60}H_{36}$ in the frequency ranges 180–390 cm^{-1} (a) and 440–560 cm^{-1} (b). Different open (solid) symbols correspond to increasing (decreasing) pressure in different pressure runs. Solid lines represent linear least-square fits. The shaded areas at $P \sim 0.6$ and $P \sim 6.0$ GPa denote the regions of possible phase transitions

may result in additional pressure-induced broadening of these peaks, which gradually obscures the initially sharp Raman structure. A similar broadening of the Raman spectra at high pressure was also observed in the isomeric mixture of C_{84} fullerene samples [22]. It is important to note that this kind of broadening is expected to be reversible with pressure, and this behavior is indeed observed in our experiments. Bearing in mind that the number of the main C–H Raman modes of $C_{60}H_{36}$ does not change with pressure, we have fitted the experimental data in this region by keeping the same number of peaks at any pressure. The pressure behavior obtained in this way is displayed in Fig. 6, in which open (solid) circles denote increasing (decreasing) pressure runs. Despite the crudeness of the procedure, the pressure dependences of the C–H Raman peak positions show a behavior that is compatible with that of the Raman modes of the fullerene molecular cage up to approximately 6 GPa. In particular, these peaks exhibit an overall positive shift up to approximately 6 GPa as well as changes in the slopes of the pressure behavior of the Raman mode frequencies at approximately 0.6 GPa. However, their pressure dependence is different for pressures above 6 GPa, where a softening in the C–H stretching vibrations is observed. It is important to note that even if we follow the pressure dependence of the «center-of-gravity» frequency of the overall C–H Raman band region, we also find a change in the slope of the pressure dependence at approximately 6 GPa. This dependence is shown in Fig. 6 by solid stars, which represent both the pressure increase and decrease runs.

The observed peculiarities in the pressure dependence of the Raman modes of $C_{60}H_{36}$ may be understood by invoking the corresponding behavior of pristine C_{60} and C_{70} at high pressure. It is known that under hydrostatic pressure at room temperature, C_{60} transforms, at 0.4 GPa or by cooling down to 259 K, from the FCC-structure, where the C_{60} molecules are orientationally disordered due to chaotic rotations, to

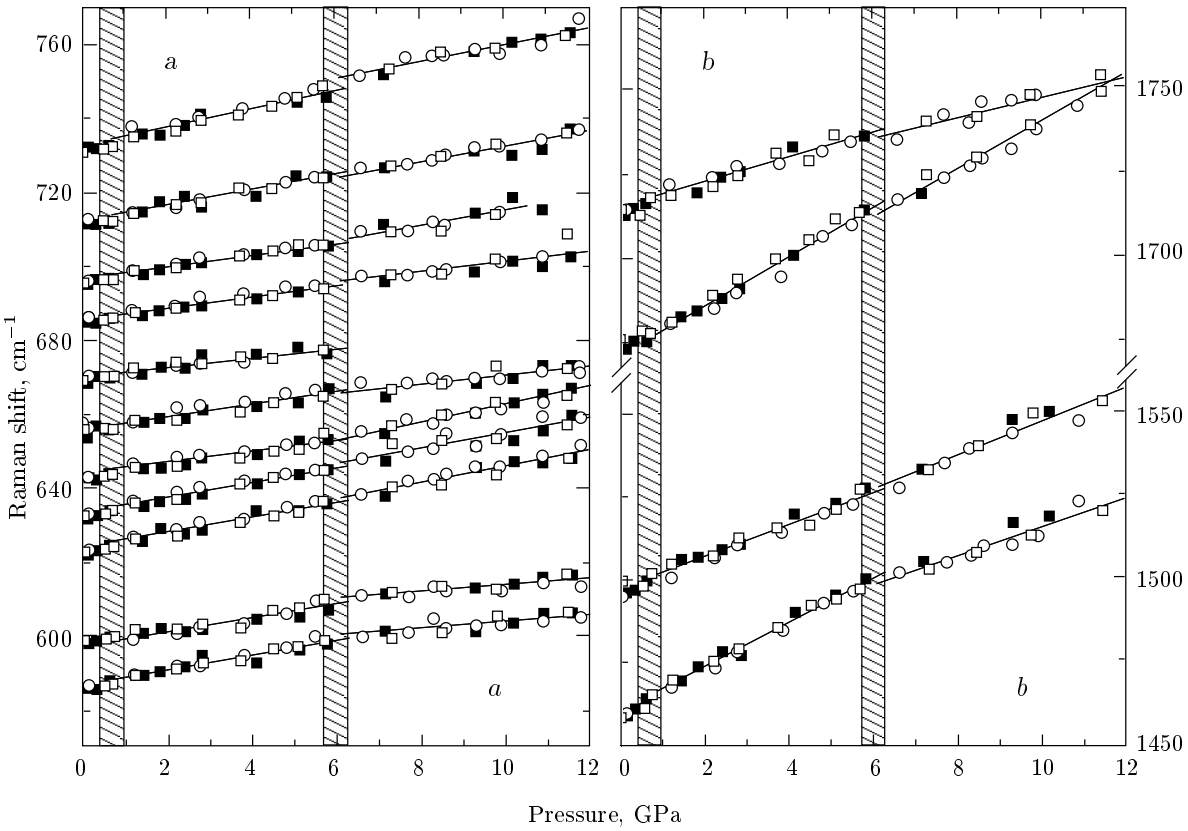

Fig. 5. Pressure dependence of Raman-active modes of $C_{60}H_{36}$ in the frequency ranges 570–770 cm^{-1} (a) and 1450–1770 cm^{-1} (b). Different open (solid) symbols correspond to increasing (decreasing) pressure in different pressure runs. Solid lines represent linear least-square fits. The shaded areas at $P \sim 0.6$ and $P \sim 6.0$ GPa denote the regions of possible phase transitions

the SC-structure, where the molecular rotations are partially ordered [23, 24]. Similarly, under pressure, C_{70} undergoes an orientational ordering phase transition from an FCC-structure to a rhombohedral phase at approximately 0.35 GPa or by cooling to 280 K [25, 26]. Furthermore, Hall et al. [9] found that the distortion of the molecules brought about by hydrogenation along with the hydrogen atoms bonded around the equator gives the molecule a strongly oblate shape. The BCC-structure allows effective packing of oblate spheroids if the polar axes of the molecules are aligned. The longer second-nearest-neighbor distance then prevents close approaches of the equatorial hydrogen atoms. If this alignment actually occurs, then there should be a tendency to form a tetragonal structure with a ratio $c/a < 1$. Therefore, they predict that at sufficiently low temperatures, the BCC-structure must transform into a body-centered tetragonal structure. Thus, keeping in mind the pressure-induced orientational ordering of C_{60} and C_{70} and the finding by Hall et al. [9], we might speculate that the observed peculiarity at approximately 0.6 GPa in the pressure dependence of Raman modes can be assigned to an orientation ordering structural phase transition.

The changes in the pressure dependence of the Raman frequencies at approximately 6 GPa, especially the behavior of the C–H stretching modes, could be attributed to a possible phase transition in which the hydrogen bonds may be involved. It is known that the intermolecular and intramolecular distances in fullerene become comparable at sufficiently high pressure. Therefore, the hydrogen atoms in the $C_{60}H_{36}$ molecule, which initially form terminal C–H bonds, can interact with carbon atoms belonging to neighboring molecular cages. This interaction may result in the formation of the bridging C–H–C hydrogen bonds when the decrease of the intermolecular distances becomes appropriate. As a result, the bulk modulus of the crystal increases, which is manifested by the decrease in the slope of the pressure dependence of the Raman fre-

quencies. In addition, the formation of the bridging hydrogen bonds results in some elongation of the involved terminal C–H bonds. The increase of the C–H terminal bond lengths results in mode softening, which increases with a further increase of pressure. The presence of the bridging C–D–C modes in the $C_{60}D_x$ samples was found recently even at ambient pressure by means of the NMR investigation of deuterofullerene [27]. Similar pressure behavior of hydrogen bonds was also found in other molecular materials that exhibit a softening in their C–H stretching mode frequency under pressure [28].

3.3. Pressure behavior of the photoluminescence spectra of $C_{60}H_{36}$

The photoluminescence spectra of $C_{60}H_{36}$ at normal pressure and various temperatures are depicted in Fig. 7. The spectrum at room temperature contains two broad peaks and two shoulders, located near the lower and higher energy sides of the spectrum. The structure of the PL spectrum is reminiscent of that of pristine C_{60} at room temperature, but the intensity of luminescence is considerably higher. The onset of the spectrum is located near 2.5 eV, which is higher than the onset of the PL spectrum in pristine C_{60} by approximately 1 eV [29]. As the temperature drops to 80 K and below to the liquid helium temperature, the PL spectrum becomes more resolved, as shown in Figs. 7*b* and 7*c*. The PL spectrum at the lowest temperature (10 K) contains a number of sharp and well-resolved peaks, located near its onset. The relatively high PL intensity in $C_{60}H_{36}$, in comparison to pristine C_{60}, is mainly associated with small luminescence quantum yield in pristine C_{60} due to the dipole-forbidden transitions from the lowest exited state [30]. The fine structure of the PL spectrum in $C_{60}H_{36}$ at low temperature resembles the well-developed structure in the PL spectrum of the C_{60} single crystals at the liquid helium temperature. This structure is related to the shallow defect levels [31], while the fine structure of the PL spectrum in the $C_{60}H_{36}$ may be related to the abundant isomer composition of the samples under study.

According to numerical local-density functional calculations of the electronic structure, the gap between the highest occupied molecular orbital (HOMO) and the lowest unoccupied molecular orbital (LUMO) is different for the five most stable isomers and varies between 3.84 and 3.91 eV [32]. These calculations are related to the isolated $C_{60}H_{36}$ molecule and their results should be compared with the experimental absorption

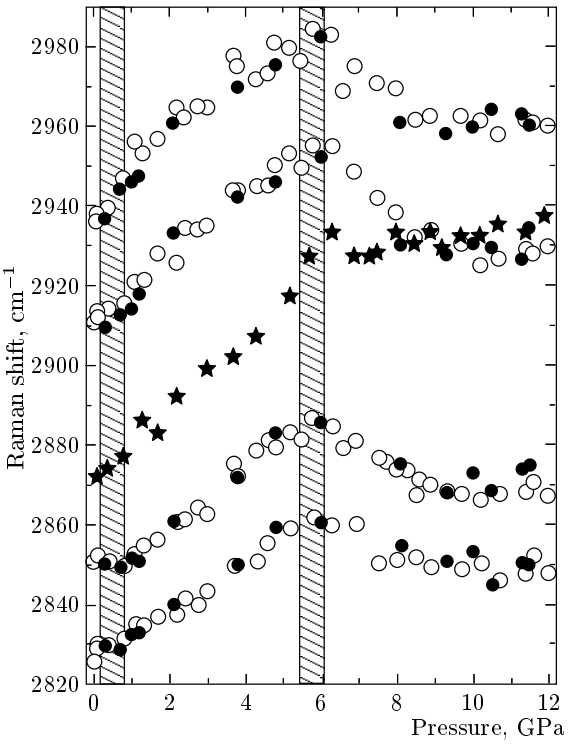

Fig. 6. Pressure dependence of the Raman-active modes of $C_{60}H_{36}$ in the range of the C–H stretching modes. Open (solid) circles correspond to the increasing (decreasing) pressure runs, while the peak positions were obtained by fitting Gaussians lineshapes to four experimental peaks at any pressure. The stars correspond to the frequency of the «center of gravity» of the C–H Raman band as a function of pressure

spectra of the $C_{60}H_{36}$ solutions. The absorption spectra of the $C_{60}H_{36}$ solutions in methylene dichloride and benzene [13] show that the onset of the absorption spectrum is located between 2.96 and 3.24 eV. Concerning the HOMO–LUMO gap calculations for the solid $C_{60}H_{36}$, there are no available data to compare with the present experimental results. As is known, the calculations of the HOMO–LUMO gap for various molecular solids show that the gap is shifted to lower energies with respect to the isolated molecules due to the vapour–crystal shift of the electron energy spectrum. In any case, the onset of the photoluminescence spectrum in solid $C_{60}H_{36}$, observed in the present work, is considerably smaller than the HOMO–LUMO gap for an isolated molecule [32].

The PL spectra of $C_{60}H_{36}$ taken at room temperature and various pressures are shown in Fig. 8. The initial spectrum taken at 0.5 GPa gradually broadens upon increase in pressure up to 12 GPa, while the shift

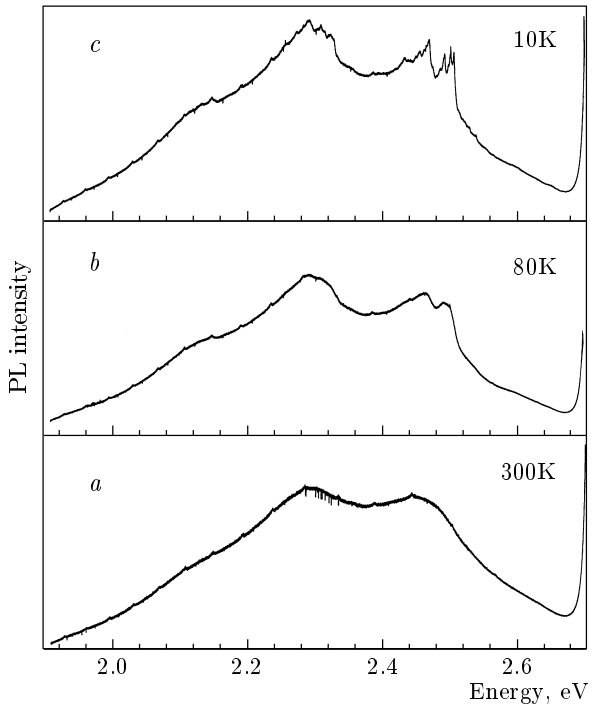

Fig. 7. Photoluminescence spectra of $C_{60}H_{36}$ at ambient pressure and various temperatures

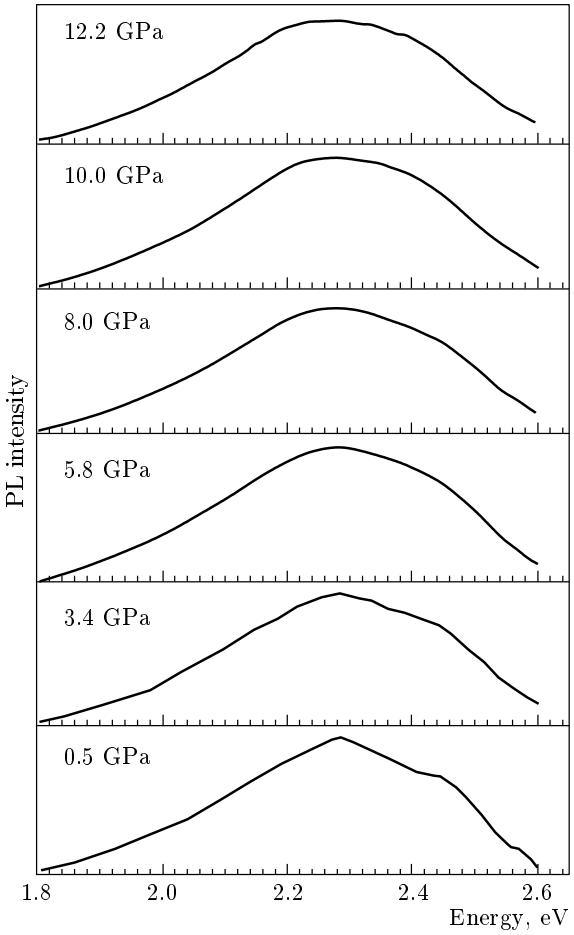

Fig. 8. Photoluminescence spectra of $C_{60}H_{36}$ at ambient temperature and various pressures

of the spectrum is not apparent. The pressure-induced shift of the spectrum is unusually small as it follows from the pressure dependence of the band frequencies obtained by fitting Gaussian band shapes to the main peaks in the PL spectrum. The pressure dependence of the two main bands of the PL spectrum of $C_{60}H_{36}$ is shown in Fig. 9. The pressure coefficients for these bands are close to zero at pressure up to approximately 6.5 GPa, but they increase in the absolute value at higher pressures, to -7.5 meV/GPa and -9 meV/GPa, respectively. The pressure behavior of the electronic states in $C_{60}H_{36}$ is not typical of molecular crystals, whose electronic levels usually exhibit large negative pressure shifts, rapidly decreasing with pressure [33]. It is known that the pressure-induced shift of the electronic levels in molecular crystals is negative for the majority of the materials that have a center of symmetry, whereas it may be positive for materials in which the molecules do not have a center of symmetry [34]. The samples under study contain the T isomer in abundance, which does not have a center of symmetry. This means that at least a part of the PL spectrum related to this isomer may have a positive pressure-induced shift, while at the same time, we have a negative pressure-induced shift originating from isomers having a center of symmetry. The unusual pressure behavior up to 6.5 GPa may be associated with mutual compensation of the opposite shifts from the two parts of the luminescence spectrum, originating from electronic states of various isomers. At higher pressure, however, the luminescence related to isomers that have a center of symmetry dominates: their electronic states are downshifted to lowest positions in energy, and we therefore have an overall negative pressure shift.

4. CONCLUSIONS

The Raman spectrum of hydrofullerene $C_{60}H_{36}$ prepared by high-pressure hydrogenation has a very rich structure and contains about five times more peaks than that of transfer-hydrogenated $C_{60}H_{36}$. The comparison of experimental Raman peaks with the results of the molecular dynamics calculation shows the presence of five principal isomers in the samples under study. The majority of the experimentally observed

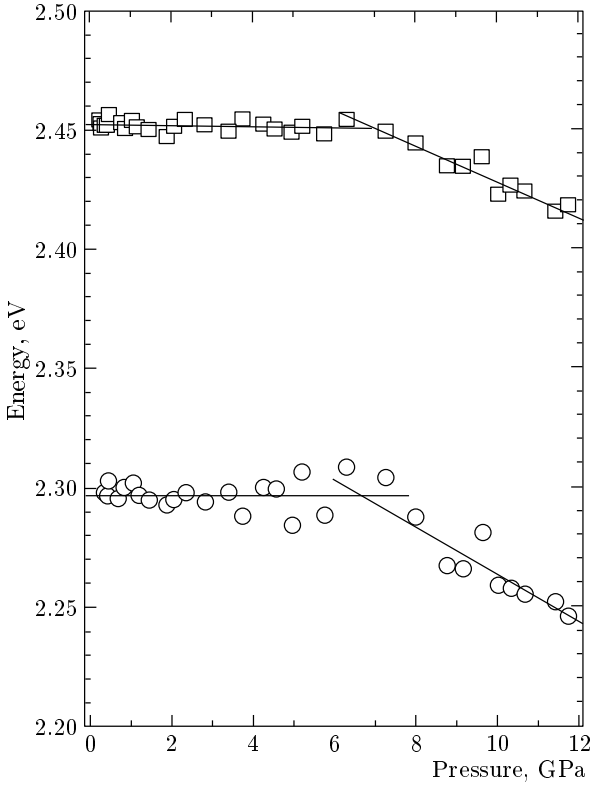

Fig. 9. Pressure dependence of the two main bands in the PL spectrum of $C_{60}H_{36}$

Raman peaks belong to the S_6, T, and D_{3d} isomers. The micro-Raman probing of several samples, prepared under different reaction parameters, shows that the homogeneity of the samples depends strongly on the reaction temperature. The Raman spectrum of deuterofullerene $C_{60}D_{36}$ prepared by the same method is in general similar to that of $C_{60}H_{36}$. The important difference between the two spectra is a large isotopic shift of the C–D stretching modes with respect to the corresponding C–H ones. The isotopic shift in the modes associated with the fullerene molecular cage is very small. This is a strong indication that the hydrogen atoms do not play an important role in the $C_{60}H_{36}$ molecular cage vibrations.

The pressure behavior of the optical Raman and PL spectra of $C_{60}H_{36}$ is not typical of fullerene-based materials because they become rather diffuse, even at relatively small pressure. The pressure dependence of the phonon frequencies is reversible with pressure and exhibits peculiarities at approximately 0.6 GPa and 6 GPa. The first peculiarity is probably related to a phase transition from the initial orientationally disordered BCC-structure to an orientationally ordered structure. The peculiarity at approximately 6 GPa may be related to a pressure-driven enhancement of the C–H interaction between the hydrogen and carbon atoms belonging to neighboring molecular cages.

The PL spectrum of $C_{60}H_{36}$ is shifted to higher energy by about 1 eV with respect to that of pristine C_{60}. The spectrum at room temperature consists of two broad peaks and becomes more structured at 10 K. The pressure-induced shift of the PL spectrum of $C_{60}H_{36}$ is close to zero up to 6.5 GPa, while at higher pressure, a negative pressure shift was observed. The unusual pressure behavior of the PL spectrum is related to the isomer composition of the high-pressure hydrogenated fullerene samples.

The authors thank S. Assimopoulos for assistance and I. O. Bashkin for providing the $C_{60}H_{36}$ samples. K. P. M. acknowledges the hospitality of the Aristotle University of Thessaloniki. Support by the RFBR, grant № 03-02-16011, and by the Russian State Research Program «Physical properties of the carbon-based nanostructures and development of new electronic devices», grant № 541-02, is gratefully acknowledged.

REFERENCES

1. A. C. Dillon, K. M. Jones, T. A. Bekkedahl, C. H. Kiang, D. S. Bethune, and M. J. Heben, Nature **386**, 377 (1997).

2. A. Rathna and J. Chandrasekhar, Chem. Phys. Lett. **206**, 217 (1993).

3. L. D. Book and G. E. Scuseria, J. Phys. Chem. **98**, 4283 (1994).

4. M. I. Attalla, A. M. Vassallo, B. N. Tattam, and J. Hamma, J. Phys. Chem. **97**, 6329 (1993).

5. I. O. Baskin, A. I. Kolesnikov, V. E. Antonov, E. G. Ponyatovsky, A. P. Kobzev, A. Y. Muzychka, A. P. Moravsky, F. E. Wagner, and G. Grosse, Mol. Mat. **10**, 265 (1998).

6. R. A. Assink, J. E. Schirber, D. A. Loy, B. Morosin, and G. A. Carlson, J. Mater. Res. **7**, 2136 (1992).

7. R. E. Haufler, J. Conceicao, P. Chibante et al., J. Phys. Chem. **94**, 8634 (1990).

8. C. Jin, R. Hettich, R. Compton, D. Joyce, J. Ble, and T. Burch, J. Phys. Chem. **98**, 4215 (1994).

9. L. E. Hall, D. R. McKenzie, M. I. Attalla, A. M. Vassallo, R. L. Davis, J. B. Dunlop, and D. J. H. Cockayne, J. Phys. Chem. **97**, 5741 (1993).

10. R. L. Davis, D. R. McKenzie, L. E. Hall, A. M. Vassallo, and A. K. Soper, ISIS Annual Report Vol. 2, Rutherford Appleton Laboratory Report RAL-94-050, p. A 200 (1994).

11. M. Bühl, W. Thiel, and U. Schneider, J. Amer. Soc. **117**, 4623 (1995).

12. R. Bini, J. Ebenhoch, M. Fanti, P. W. Fowler, S. Leach, G. Orlandi, C. Ruchardt, J. P. B. Sandall, and F. Zerbetto, Chem. Phys. **232**, 75 (1998).

13. R. V. Bensasson, T. J. Hill, E. J. Land, S. Leach, D. J. McGarvey, T. G. Truscott, J. Ebenhoch, M. Gerst, and C. Rüchardt, Chem. Phys. **215**, 111 (1997).

14. A. D. Darwish, A. K. Abdul-Sada, G. J. Langley, H. W. Kroto, R. Taylor, and D. R. Walton, J. Chem. Soc. Perkin Trans. **2**, 2359 (1995).

15. Y. Iwasa, T. Arima, R. M. Fleming, T. Siegrist, O. Zhou, R. C. Haddon, L. J. Rothberg, K. B. Lyons, H. L. Carter Jr., A. F. Hebard, R. Tycko, G. Dabbagh, J. J. Krajewski, G. A. Thomas, and T. Yagi, Science **264**, 1570 (1994).

16. S. K. Konovalov and B. M. Bulychev, Zh. Neorg. Khim. **37**, 2640 (1992).

17. A. Jayaraman, Rev. Sci. Instr. **57**, 1013 (1986).

18. D. Barnett, S. Block, and G. J. Piermarini, Rev. Sci. Instr. **44**, 1 (1973).

19. D. S. Bethune, G. Meijer, W. C. Tang, H. J. Rosen, W. G. Golden, H. Seki, C. A. Brown, and M. S. De Vries, Chem. Phys. Lett. **179**, 181 (1991).

20. B. W. Clare and D. L. Kepert, J. Mol. Struct. (Theochem.) **315**, 71 (1994).

21. K. Ushizawa, M. N.-Gamo, Y. Kikuchi, I. Sakogushi, V. Sato, and T. Ando, Phys. Rev. B, **60**, R5165 (1999).

22. I. Margiolaki, S. Margadona, K. Prassides, S. Assimopoulos, I. Tsilika, K. P. Meletov, G. A. Kourouklis, T. J. S. Dennis, and H. Shinohara, Physica B **318**, 372 (2002).

23. G. A. Samara, J. E. Schirber, B. Morosin, L. V. Hansen, D. Loy, and D. Sylwester, Phys. Rev. Lett. **67**, 3136 (1991).

24. K. P. Meletov, G. Kourouklis, D. Christofilos, and S. Ves, Phys. Rev. B **52**, 10090 (1995).

25. C. Christides, I. M. Thomas, T. J. Dennis, and K. Prassides, Europhys. Lett. **22**, 611 (1993).

26. A. Lundin, A. Soldadov, and B. Sunquist, Europhys. Lett. **30**, 469 (1995).

27. V. P. Tarasov, Y. B. Muravlev, V. N. Fokin, and Y. M. Shulga, Appl. Phys. A **78**, 1001 (2004).

28. E. Katoh, H. Yamawaki, H. Fujihisa, M. Salashita, and K. Aoki, Phys. Rev. B **59**, 11244 (1999).

29. K. P. Meletov, D. Christofilos, S. Ves, and G. A. Kourouklis, Phys. Stat. Sol. (b) **198**, 553 (1996).

30. P. A. Lane, L. S. Swanson, Q.-X. Ni, J. Shinar, J. P. Engel, T. J. Barton, and L. Jones, Phys. Rev. Lett. **68**, 887 (1992).

31. W. Guss, J. Feldman, E. O. Göbel, C. Taliani, H. Mohn, W. Müller, P. Häussler, and H.-U. ter Meer, Phys. Rev. Lett. **72**, 2644 (1994).

32. B. I. Dunlap, D. W. Brenner, and G. W. Schriver, J. Phys. Chem. **98**, 1756 (1994).

33. K. P. Meletov, V. K. Dolganov, O. V. Zharikov, I. N. Kremenskaya, and Yu. A. Ossipyan, J. de Phys. I **2**, 2097 (1992).

34. A. S. Davydov, *Theory of Molecular Excitons*, Plenum Press, New York (1971).

35. K. P. Meletov, G. A. Kourouklis, D. Christophilos, and S. Ves, JETP **81**, 798 (1995).